Appl. Math. Mech. -Engl. Ed., **39**(3), 395–408 (2018)

Applied Mathematics and Mechanics (English Edition)

https://doi.org/10.1007/s10483-017-2307-7

Fluid flow driven along microchannel by its upper stretching wall with electrokinetic effects*

Hang XU[1], I. POP[2], Q. SUN[3,†]

1. Collaborative Innovation Center for Advanced Ship and Deep-Sea Exploration, State Key Lab of Ocean Engineering, School of Naval Architecture, Ocean and Civil Engineering, Shanghai Jiao Tong University, Shanghai 200240, China;
2. Department of Mathematics, Babeş-Bolyai University, Cluj-Napoca 400084, Romania;
3. Particulate Fluids Processing Centre, Department of Chemical Engineering, The University of Melbourne, Parkville, VIC 3010, Australia

(Received Jul. 13, 2017 / Revised Aug. 31, 2017)

Abstract We develop a mathematical model to describe the flow in a microchannel driven by the upper stretching wall of the channel in the presence of electrokinetic effects. In this model, we avoid imposing any unphysical boundary condition, for instance, the zero electrostatic potential in the middle of the channel. Using the similarity transformation, we employ the homotopy analysis method (HAM) to get the analytical solution of the model. In our approach, the unknown pressure constant and the integral constant related to the electric potential are solved spontaneously by using the proper boundary conditions on the channel walls, which makes our model consistent with the commonly accepted models in the field of fluid mechanics. It is expected that our model can offer a general and proper way to study the flow phenomena in microchannels.

Key words microchannel, electrokinetic effect, stretching wall, electro-viscous flow model

Chinese Library Classification O361
2010 Mathematics Subject Classification 76D05, 76M55, 65D99

1 Introduction

Fluid flow in microchannels has been recognised as a major role in the applications of micro-electro-mechanical systems (MEMS) and microfluidics, for instance, microchannel heat sinks for cooling microchips and laser diode arrays[1–2], lab-on-chip devices for chemical and biomedical analyses[3], and microfluid pumps[4]. Several theoretical and experimental studies have been performed towards understanding the fundamental transport mechanisms of microchannel flow. Among them, Eringen[5] suggested a simple model in which he described the fluid flow in the microchannels by using the Navier-Stokes equations with jump conditions. Pfahler et

* Citation: Xu, H., Pop, I., and Sun, Q. Fluid flow driven along microchannel by its upper stretching wall with electrokinetic effects. *Applied Mathematics and Mechanics* (*English Edition*), **39**(3), 395–408 (2018) https://doi.org/10.1007/s10483-017-2307-7

† Corresponding author, E-mail: qiang.sun@unimelb.edu.au

al.[6] observed that the predictions by the Navier-Stokes equations are in agreement with the experimental results to some extent for the flow in the large channels, but different from the experimental data of the flow within small ones. Mala et al.[7–8] discovered that the influence of the electric double layer (EDL) at the solid-liquid interface on the flow in a microchannel has to be considered to make the theoretical results consistent with the experimental ones. Ren et al.[9] found that it is necessary to address the additional flow resistance due to the electrokinetic effect in microchannels. Their theoretical analysis based on the electro-viscous flow models gave better agreement with the experimental results compared with those by the Navier-Stokes equations.

It is worth mentioning that the electro-viscous flow model used by Mala et al.[7–8] employed an arbitrary boundary condition to force the electrostatic potential ϕ in the middle of the microchannel to be 0, which leads to the fact that both the electrostatic potential and the flow velocity profiles in the microchannel are not physical. Moreover, the mathematical model for flow field used by Mala et al.[7–8] as well as that by Ren et al.[9] contains a constant pressure parameter whose value was set to be known from the experimental data. Though it significantly simplified the procedure to obtain results with acceptable accuracies, it is far from being a correct way to develop mathematical models for the flow in microchannels. Theoretically, as has been discussed in detail in the literature[10–19], this pressure parameter has to be taken as an unknown constant to be calculated based on the boundary conditions.

In this paper, we develop a theoretical model of the liquid flow in a microchannel driven by its upper moving wall together with the effects of the EDL. Compared with the models used by Mala et al.[7–8] and Ren et al.[9] for the flow in the microchannel due to the pressure difference, two drawbacks have been overcome in our model. Firstly, we remove the unphysical artificial zero electric potential condition in the middle of the microchannel. Secondly, we calculate the unknown pressure constant in the model by using the boundary conditions on the microchannel walls, which makes our model consistent with the models that are commonly employed in the field of fluid mechanics to describe the channel flow. After this short introduction section, we describe the flow model for the microchannel flow due to the moving wall together with the electric double layer effect in detail in Section 2 and Section 3. We then give the detailed procedure to find the analytical solution of the governing equation by using the homotopy analysis method (HAM)[20] in Section 4 that is also validated with the numerical results obtained by the finite difference technology[21]. The flow phenomena are studied under different flow conditions in Section 5, which is followed by a short conclusion in Section 6.

2 Analytical solution of electrostatic potential

Consider a fluid flow between two horizontally parallel flat plates separated by a small distance H, as shown in Fig. 1. In practice, the liquid usually is a dilute solution that contains positive and negative ions. Also, the walls of the microchannel are commonly slightly charged. When the flow channel is small, the electrostatic effects on the flow cannot be ignored. In our model, we set that the electric potentials on both surfaces are identical and reduce gradually into fluid. The concentration of the suspended ions is uniform in the channel. In the vicinity of the surfaces the electrostatic potential ϕ at any point is associated with the net number of electrical charges per unit volume ρ_{e}, which can be expressed, based on the theory of electrostatics, in the following form:

$$\frac{\mathrm{d}^2\phi}{\mathrm{d}y^2} = -\frac{\rho_{\mathrm{e}}(y)}{\varepsilon_0\varepsilon}, \tag{1}$$

where ε and ε_0 are, respectively, the dielectric constant of the fluid and the permittivity of vacuum.

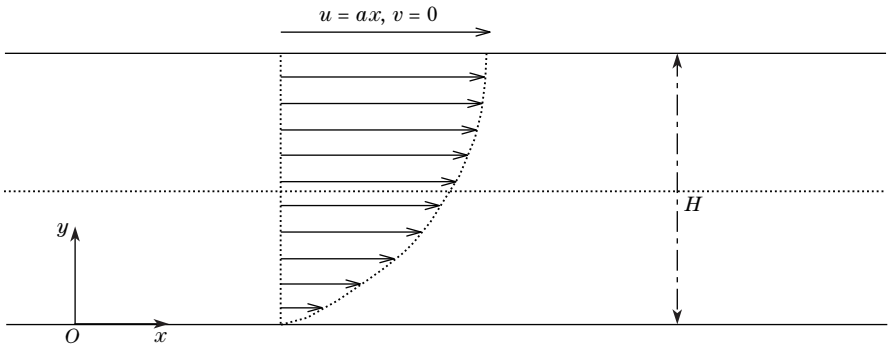

Fig. 1 Physical model and coordinate system for flow in microchannel that is driven by moving upper wall of channel together with effects of electrostatic double layer

Invoking the equilibrium Boltzmann distribution, in which the uniform dielectric constant is applicable, the solution of the number of ion distribution in a symmetric electrolyte can be then written as

$$n_i = n_{0i} \exp\Big(- \frac{\widehat{z}_i \, e \, \phi(y)}{k_\mathrm{b} \widehat{T}} \Big), \tag{2}$$

where n_{0i} is the bulk ionic concentration, $\widehat{z}_i$ is the valence of type i ions, e is the fundamental charge, k_b is the Boltzmann's constant, and $\widehat{T}$ is the absolute temperature. The net charge density in a unit volume of the fluid is defined by

$$\rho_\mathrm{e}(y) = (n^+ - n^-) \, \widehat{z} \, e = -2 \, n_0 \, \widehat{z} \, e \, \sinh\Big(\frac{\widehat{z} \, e \, \phi(y)}{k_\mathrm{b} \, \widehat{T}} \Big). \tag{3}$$

Substituting Eq. (3) into the Poisson equation (1), we obtain

$$\frac{\mathrm{d}^2 \phi}{\mathrm{d}y^2} = \frac{2 \, n_0 \, \widehat{z} \, e}{\varepsilon_0 \, \varepsilon} \sinh\Big(\frac{\widehat{z} \, e \, \phi(y)}{k_\mathrm{b} \, \widehat{T}} \Big). \tag{4}$$

By using the dimensionless variables

$$\Phi(\eta) = \frac{\widehat{z} \, e \, \phi(y)}{k_\mathrm{b} \, \widehat{T}}, \quad \Theta(\eta) = \frac{\rho_\mathrm{e}(y)}{n_0 \, \widehat{z} \, e}, \quad \eta = \frac{y}{H}, \tag{5}$$

Eq. (1) and Eq. (4) are simplified to

$$\Phi''(\eta) = \kappa^2 \sinh(\Phi(\eta)), \tag{6}$$

$$\Phi''(\eta) = -\frac{\kappa^2}{2} \Theta(\eta), \tag{7}$$

where $\kappa = H \, k$ is a dimensionless constant with $k = (2 \, n_0 \, \widehat{z}^2 \, e^2 / (\varepsilon_0 \, \varepsilon \, k_\mathrm{b} \, \widehat{T}))^{1/2}$ being the reciprocal of the Debye length. When the electrical potential is small compared with the thermal energy of the ions, $|\widehat{z} e \phi| < |k_\mathrm{b} \widehat{T}|$, Eq. (6) can be linearized to the Debye-Hückel model as follows:

$$\Phi''(\eta) = \kappa^2 \Phi(\eta). \tag{8}$$

The appropriate boundary conditions for the dimensionless electrostatic potential Φ are

$$\Phi(0) = \Phi(1) = \overline{\zeta} = \frac{\widehat{z} e \zeta}{k_\mathrm{b} \widehat{T}}, \tag{9}$$

where ζ denotes the measurable electrical potential between the boundaries of the compact layer and the diffuse layer of the EDL at the shear plates.

When using the boundary conditions in Eq. (9), the closed-form solution of Eq. (8) is

$$\Phi(\eta) = \frac{\overline{\zeta}}{1+\exp(\kappa)}\exp(\kappa\eta) + \frac{\overline{\zeta}}{1+\exp(-\kappa)}\exp(-\kappa\eta). \tag{10}$$

3 Equations of fluid motion

To describe the fluid flow motion between two parallel flat plates driven by its upper stretching plate with the effects of the EDL, as displayed in Fig. 1, the following assumptions are imposed: the fluid is incompressible, the flow is laminar and steady, and the velocity of the flow away from the channel walls is independent of position along the x-direction. When the viscous force, the pressure force, and the electrical body force generated by the double layer electric field are all considered, the Navier-Stokes equations to describe this microchannel flow can be written as

$$\frac{\partial u}{\partial x} + \frac{\partial v}{\partial y} = 0, \tag{11}$$

$$u\frac{\partial u}{\partial x} + v\frac{\partial u}{\partial y} = -\frac{1}{\rho_{\mathrm{f}}}\frac{\partial p}{\partial x} + \nu_{\mathrm{f}}\Big(\frac{\partial^2 u}{\partial x^2} + \frac{\partial^2 u}{\partial y^2}\Big) + \frac{E_x\rho_{\mathrm{e}}}{\rho_{\mathrm{f}}}, \tag{12}$$

$$u\frac{\partial v}{\partial x} + v\frac{\partial v}{\partial y} = -\frac{1}{\rho_{\mathrm{f}}}\frac{\partial p}{\partial y} + \nu_{\mathrm{f}}\Big(\frac{\partial^2 v}{\partial x^2} + \frac{\partial^2 v}{\partial y^2}\Big). \tag{13}$$

The boundary conditions are

$$\begin{cases} u = 0, \quad v = 0 \quad \text{at} \quad y = 0, \\ u = u_{\mathrm{w}} = a\,x, \quad v = 0 \quad \text{at} \quad y = H, \end{cases} \tag{14}$$

where u and v are the velocity components along the x-axis and y-axis, respectively, p denotes the pressure, ρ_{f} is the fluid density, ν_{f} is the kinematic viscosity, and E_x is the electric field strength.

Define the following similarity transformations:

$$\psi(x,y) = (ax)HF(\eta), \quad \eta = \frac{y}{H}, \tag{15}$$

where $\psi(x,y)$ is the stream function,

$$u = \frac{\partial\psi}{\partial y}, \quad v = -\frac{\partial\psi}{\partial x}. \tag{16}$$

Substituting Eq. (15) into Eqs. (11), (12), and (13), the continuity equation (11) is satisfied straightforwardly, and the rest of equations can be written, by emphasizing the pressure related terms, as follows:

$$\frac{1}{\rho_{\mathrm{f}}}\frac{\partial p}{\partial x} = a^2 x\Big(\frac{\nu_{\mathrm{f}}}{aH^2}F''' + F\,F'' - F'^2 + \frac{E_x\rho_{\mathrm{e}}}{\rho_{\mathrm{f}}a^2x}\Big), \tag{17}$$

$$\frac{1}{\rho_{\mathrm{f}}}\frac{\partial p}{\partial y} = a^2 H\Big(FF' - \frac{\nu_{\mathrm{f}}}{aH^2}F''\Big). \tag{18}$$

Since the terms on the right-hand side of Eq. (18) are independent of x, which indicates

$$\frac{\partial^2 p}{\partial x\partial y} = 0.$$

As a result, we obtain

$$\frac{1}{Re}F''' + F\,F'' - F'^2 + \frac{E_x\rho_{\rm e}}{\rho_{\rm f}a^2x} = K, \tag{19}$$

where

$$Re = aH^2/\nu_{\rm f}$$

is the Reynolds number, and K is the pressure constant to be determined.

To obtain the electric field strength E_x, we quantify the balance between the streaming current and the electrical conduction current[7–8]. As it is known that in the absence of an applied electric field, when a dilute solution is forced through a channel under hydrostatic pressure, the streaming current is generated, which can be expressed as

$$I_{\rm s} = \int_{A_{\rm c}} u\rho_{\rm e}{\rm d}A_{\rm c}, \tag{20}$$

where $A_{\rm c}$ is the cross-sectional area of the flow channel.

The streaming potential further produces a conduction current in the reverse direction which is

$$I_{\rm c} = \frac{\lambda_0 E_{\rm s} A_{\rm c}}{L}, \tag{21}$$

where λ_0 is the electrical conductivity of the fluid, $E_{\rm s}$ is the streaming potential, and L is a reference length of the channel.

At the steady state, the net electrical current is zero, i.e.,

$$I = I_{\rm s} + I_{\rm c} = 0. \tag{22}$$

Substituting Eq. (15) into Eqs. (20) and (21), we obtain

$$I_{\rm s} = \int_{A_{\rm c}} u\,\rho_{\rm e}\,{\rm d}A_{\rm c} = -2n_0\widehat{z}eWHax\int_0^1 F'\Phi\,{\rm d}\eta, \tag{23}$$

$$I_{\rm c} = \frac{\lambda_0 E_{\rm s} A_{\rm c}}{L} = E_x\lambda_0 WH, \tag{24}$$

where W is the reference width of the channel and $E_x = E_{\rm s}/L$. Solving Eq. (22), we obtain

$$E_x = \frac{2an_0\widehat{z}e}{\lambda_0}x\int_0^1 F'\Phi{\rm d}\eta. \tag{25}$$

Therefore, the last term on the left-hand side of Eq. (19) can be written as

$$\frac{E_x\rho_{\rm e}}{\rho_{\rm f}a^2x} = -G_1\Phi\int_0^1 F'\Phi{\rm d}\eta, \tag{26}$$

where

$$G_1 = \frac{2n_0\widehat{z}e}{\lambda_0\rho_{\rm f}a}$$

is a dimensionless constant.

Using Eq. (26), Eq. (19) can then be reduced to

$$\frac{1}{Re}F''' + FF'' - F'^2 - G_1\Big(\int_0^1 F'(\eta)\,\Phi(\eta){\rm d}\eta\Big)\Phi(\eta) = K \tag{27}$$

with the boundary conditions

$$F(0)=0,\quad F'(0)=0,\quad F(1)=0,\quad F'(1)=1. \tag{28}$$

Two physical parameters are important to quantify the flow phenomena in the microchannels and for the engineering design of microchannels, namely, the local skin frictional coefficients on both walls. We give the definitions of these two parameters before showing the detailed solution procedure of Eq. (27):

$$C_{fx\mathrm{l}}=\frac{\tau_{\mathrm{wl}}}{\rho_{\mathrm{f}}\,u_{\mathrm{w}}^2},\quad C_{fx\mathrm{u}}=\frac{\tau_{\mathrm{wu}}}{\rho_{\mathrm{f}}\,u_{\mathrm{w}}^2}, \tag{29}$$

where

$$\tau_{\mathrm{wl}}=\mu_{\mathrm{f}}\frac{\partial u}{\partial y}\Big|_{y=0},\quad \tau_{\mathrm{wu}}=\mu_{\mathrm{f}}\frac{\partial u}{\partial y}\Big|_{y=1}. \tag{30}$$

Substituting Eq. (30) into Eq. (29), we obtain

$$C_{fx\mathrm{l}}=\frac{1}{Re}\Big(\frac{1}{\xi}\Big)F''(0),\quad C_{fx\mathrm{u}}=\frac{1}{Re}\Big(\frac{1}{\xi}\Big)F''(1), \tag{31}$$

where $\xi=x/H$ is the dimensionless length variable.

4 Solution method

It is worth noting that Eq. (27) contains two unknown constants K and $\int_0^1 F'(\eta)\,\Phi(\eta)\mathrm{d}\eta$ which are difficult to be calculated accurately during the solution finding procedure by numerical or analytical approaches without particular treatments. Nevertheless, in this work, we employ and extend the HAM technique to obtain the exact solution of the nonlinear equation (27) subject to the boundary conditions in Eq. (28), in which the exact values of the unknown constants, K and $\int_0^1 F'(\eta)\,\Phi(\eta)\mathrm{d}\eta$, are calculated spontaneously and simultaneously as parts of the solution procedure without any particular tricks.

We first write the unknown constants K and $\int_0^1 F'(\eta)\,\Phi(\eta)\mathrm{d}\eta$ as

$$K=\sigma_0+\sum_{j=1}^{\infty}\sigma_j,\quad \int_0^1 F'(\eta)\,\Phi(\eta)\mathrm{d}\eta=\omega_0+\sum_{j=1}^{\infty}\omega_j, \tag{32}$$

and then express the functions $F(\eta)$ and $\Phi(\eta)$ as

$$F(\eta)=f_0(\eta)+\sum_{j=1}^{\infty}f_j(\eta),\quad \Phi(\eta)=\phi_0(\eta)+\sum_{j=1}^{\infty}\phi_j(\eta). \tag{33}$$

In the framework of the HAM, the kth order HAM deformation equations can be written as

$$f_m'''-\chi_m f_{m-1}'''=\hbar_{\mathrm{f}}\,R_{f,\,m}, \tag{34}$$

$$\phi_m''-\chi_m\phi_{m-1}''=\hbar_{\phi}\,R_{\phi,\,m} \tag{35}$$

with the boundary conditions

$$f_m(0)=0,\quad f_m'(0)=0,\quad f_m(1)=0,\quad f_m'(1)=0,\quad \phi_m(0)=0,\quad \phi_m(1)=0, \tag{36}$$

where $\hbar_{\mathrm{f}}$ and $\hbar_\phi$ are the HAM auxiliary parameters used for the convergence-control of the HAM analytical approximations. Also, $R_{f,\,m}$, $R_{\phi,\,m}$, and χ_m are defined, respectively, by

$$R_{f,\,m} = \frac{1}{Re} f'''_{m-1} + \sum_{j=0}^{m-1} (f_j\, f''_{m-1-j} - f'_j\, f'_{m-1-j} - G_1\, \omega_j\, \phi_{m-1-j}) - \sigma_{m-1}, \tag{37}$$

$$R_{\phi,\,m} = \phi''_{m-1} - \kappa^2 \phi_{m-1}, \tag{38}$$

and

$$\chi_m = \begin{cases} 0, & m \leqslant 1, \\ 1, & m > 1. \end{cases} \tag{39}$$

The solutions of Eqs. (34) and (35) are in the forms of

$$f_m = f^* + \chi_m\, f_{m-1} + C_{0,\,m} + C_{1,\,m}\, \eta + C_{2,\,m}\, \eta^2, \tag{40}$$

$$\phi_m = \phi^* + \chi_m\, \phi_{m-1} + C_{3,\,m} + C_{4,\,m}\, \eta, \tag{41}$$

where

$$f^* = \iiint (\hbar_{\mathrm{f}}\, R_{f,\,m})\, \mathrm{d}\eta\, \mathrm{d}\eta\, \mathrm{d}\eta, \tag{42}$$

$$\phi^* = \iint (\hbar_\phi\, R_{\phi,\,m})\, \mathrm{d}\eta\, \mathrm{d}\eta, \tag{43}$$

and the constants $C_{i,\,m}$ $(i = 0, 1, 2, 3, 4)$ are determined by the boundary conditions

$$\begin{cases} C_{0,\,m} = -f^*_m(0), \quad C_{1,\,m} = -f'^*_m(0), \\ C_{2,\,m} = -f^*_m(1) - C_{0,\,m} - C_{1,\,m}, \\ C_{3,\,m} = \dfrac{\phi^*(1) + \phi^*(-1)}{2}, \\ C_{4,\,m} = \dfrac{\phi^*(-1) - \phi^*(1)}{2}. \end{cases} \tag{44}$$

The above HAM solution procedure can work accordingly after the initial approximations $f_0(\eta)$ and $\phi_0(\eta)$ are chosen properly based on the boundary conditions (9) and (28), such as

$$f_0(\eta) = \eta^4 - \eta^3, \quad \phi_0(\eta) = \overline{\zeta}. \tag{45}$$

During the HAM solution procedure, the unknown constant K is determined in the following way. Due to Eqs. (34) and (37), it is known that $f'_m(\eta) = 0$ contains the unknown term ω_{m-1}, which can be obtained by using the boundary condition $f'_m(1) = 0$ defined in Eq. (36). For example, for the zeroth order approximation for K when $m = 0$ in Eq. (32), as $f'_1(1) = 0$, we have

$$\frac{1}{Re} - \frac{5}{252} - \frac{1}{6}\sigma_0 = 0, \tag{46}$$

which leads to

$$\sigma_0 = \frac{252 - 5Re}{42Re}. \tag{47}$$

Also, the constant integration term $\omega_0 = \int_0^1 f'_0(\eta)\, \phi_0(\eta) \mathrm{d}\eta$ can be obtained from Eq. (45). In this way, the whole solution series in Eq. (32) for K and the constant integration term can be determined successively from $m = 1, 2, 3, \cdots$.

5 Results

To check the accuracy of our solution, we define the following error estimation formula:

$$E_{\mathrm{f}}(m)=\int_0^1\Big(\frac{1}{R}F'''+FF''-F'^2-G_1\Big(\int_0^1 F'(\eta)\,\Phi(\eta)\mathrm{d}\eta\Big)\Phi(\eta)-K\Big)^2\mathrm{d}\eta. \tag{48}$$

Substituting mth order computational results into Eq. (48), the corresponding error can be obtained. For example, for prescribed values of $Re=5$ and $G_1=10$, by properly choosing $\hbar_{\mathrm{f}}=-2$ and $\hbar_\phi=-1/2$ (Padé technique is used for $\kappa=20$), we find that the errors are perfectly small, as listed in Table 1. Also, we run a few validations between the analytic results obtained by the HAM and the results by the numerical technique, finite difference method. When applying the finite difference method to solve governing equation (27) together with the boundary conditions in Eq. (28), we first take one derivation of Eq. (27) with respect of η. Then, the central finite difference schemes are employed to represent the differential terms in the resulting governing equation, and a ghost node on each end of the computational zone is used to take care of the first order derivations in the boundary conditions. The integral term is represented by Simpson's rule. The nonlinearity of the governing equation is dealt with through iteration. As shown in Fig. 2, good agreement has been found between the analytical approximations by the HAM and the numerical results by the finite difference method.

Table 1 Computational errors with different order HAM approximations under different values of κ at $Re=5$ and $G_1=10$

Order	$\kappa=0$	$\kappa=1$	$\kappa=3$	$\kappa=5$	$\kappa=20$
0	1.453 27	1.453 27	1.453 27	1.453 27	1.453 27
10	4.33×10^{-5}	4.29×10^{-5}	4.29×10^{-5}	5.84×10^{-5}	2.40×10^{-2}
20	2.99×10^{-9}	2.87×10^{-9}	2.78×10^{-9}	1.82×10^{-8}	7.91×10^{-4}
30	2.75×10^{-13}	2.62×10^{-13}	2.52×10^{-13}	9.93×10^{-11}	1.57×10^{-5}
40	–	–	–	–	1.83×10^{-9}
50	–	–	–	–	4.39×10^{-13}

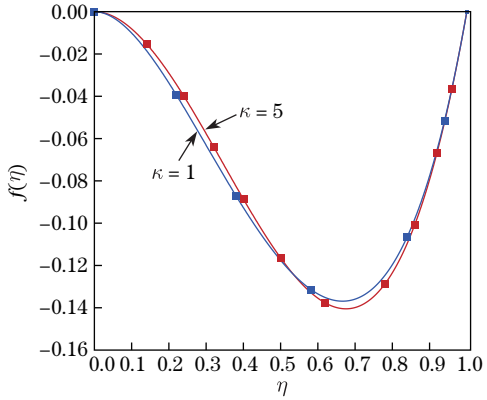

Fig. 2 Comparisons of stream function values at $Re=5$ and $G_1=50$ between 50th order analytical approximations by HAM (lines) and numerical results by finite difference method with 1 000 uniform elements (symbols) (color online)

As seen in Fig. 3, $\Phi(\eta)$ decreases monotonously as κ increases. Particularly, as κ becomes sufficiently large, $\Phi(\eta)$ diminishes to zero in the middle of the channel. This leads to the

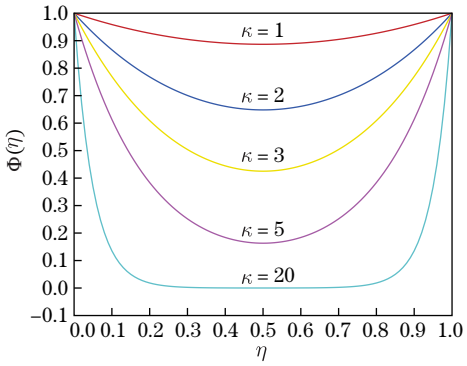

Fig. 3 Field values of electric potential $\Phi(\eta)$ under different κ

common assumptions of zeta potential[22] in the application of capillary: (i) the capillary walls are flat, and (ii) the double layer develops fully so that the potential in the middle of the capillary is zero. Traditionally, people took that $\kappa = 5$ could be large enough to describe such electrokinetic phenomena in fluid flows since the potential in the mid plane is small compared with the potential near the wall. However, Burgreen and Nakache[23] showed that the influence of the zeta potential still exists across the channel even when $\kappa = 10$ in which the distance between the two plates is already considerably large. Also, it is known that the double layer field is significant near the channel walls. For instance, the double layer occupies only 8% of the channel cross-sectional area for $\kappa = 80$.

In Fig. 4, the influences of κ on the pressure constant K are presented. From this figure, we can see that the pressure constant K decreases dramatically as κ increases when it is small. Once reaching the minimum value, K increases as κ evolves. The pressure constant K approaches to 1 as κ keeps continuously increasing. This indicates that the influence of the electrostatic potential on the pressure gradient is opposite to that caused by the upper stretching wall. κ has significant effects on K when the distance between two parallel plates is small. As the distance between the two walls consecutively increases, the electrostatic potential in the middle of the channel diminishes to zero. In this situation, the effect of the electrostatic potential on the pressure gradient becomes weaker and weaker, which results in that the effects on the pressure gradient due to the upper stretching wall of the channel become dominant.

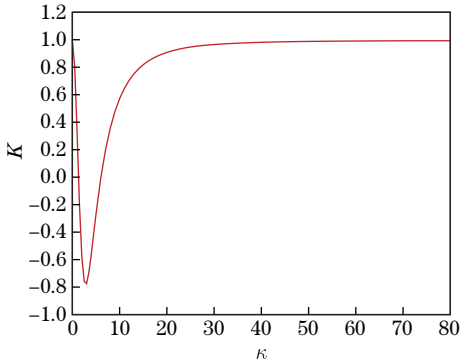

Fig. 4 Dependence of pressure constant K on κ when $Re = 5$ and $G_1 = 100$

It should be noted that, from Eq. (31), $F''(0)$ and $F''(1)$ are the core parts of the local skin friction coefficients $C_{fx\mathrm{l}}$ and $C_{fx\mathrm{u}}$, respectively. Therefore, we consider the effects of κ on $F''(0)$ and $F''(1)$ that will straightforwardly reflect the effects of κ on $C_{fx\mathrm{l}}$ and $C_{fx\mathrm{u}}$. As shown in Fig. 5, $F''(0)$ decreases rapidly as κ increases when κ is not large. After passing the minimum

value, $F''(0)$ grows with κ increasing. Physically, the double layer electric field generates an electrical body force, which is opposite to the frictional resistance. As a result, its enhancement decreases the drag resistance, while as κ is large enough, the effect of electrostatic potential becomes negligible in most part of the fluid within the microchannel. It is shown in Fig. 6 that the variation of $F''(1)$ with κ exhibits the totally reverse trend relative to that of $F''(0)$. $F''(1)$ rapidly enhances to its maximum value, then gradually reduces as κ continuously reduces. This means that the electrical body force exerts a positive influence on the skin friction coefficients for small κ, whose effect becomes weaker and weaker when the size of the channel increases. The streaming potential

$$E_{\mathrm{s}} \equiv G_1 \int_0^1 F'(\eta)\,\Phi(\eta)\mathrm{d}\eta$$

is also an important quantity to affect the flow patterns in a microchannel. As shown in Fig. 7, E_{s} develops very quickly as κ evolves. When the electrostatic potential in the middle of the microchannel just diminishes to zero, the streaming potential reaches its peak value. After that, E_{s} reduces as κ increases. Physically, the reason is that the large distance of electrokinetic separation corresponds to a large volume transport so that more ions are carried to the end of the channel which leads to a higher charge accumulation.

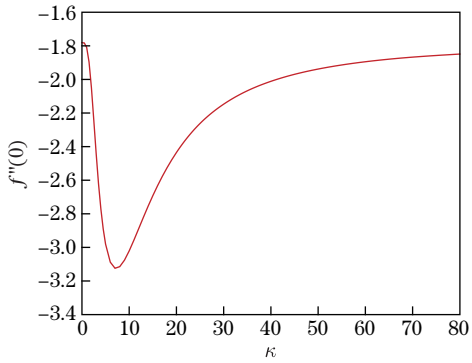

Fig. 5 Variation of $f''(0)$ for local skin frictional coefficient on lower wall along κ when $Re = 5$ and $G_1 = 100$

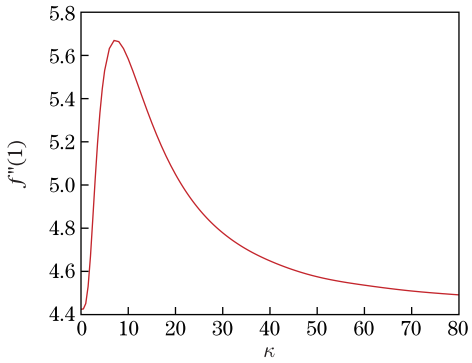

Fig. 6 Variation of $f''(1)$ for local skin frictional coefficient on upper wall along κ when $Re = 5$ and $G_1 = 100$

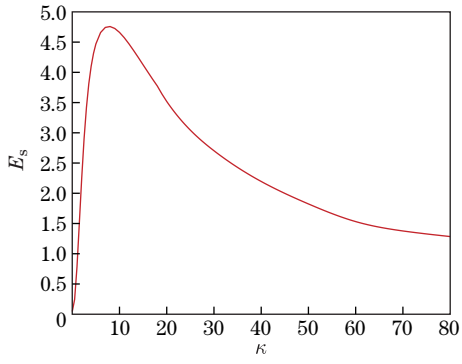

Fig. 7 Dependence of stream potential E_{s} on κ when $Re = 5$ and $G_1 = 100$

It is a common sense that the Reynolds number Re plays an important role in the flow characteristics. As shown in Fig. 8, when κ is small, K decreases dramatically as Re enlarges at first, and then it enhances slightly as Re continuously evolves. However, when κ is large (i.e., $\kappa = 20$), K decreases monotonously as Re increases. These trends show that Re plays a dominant role on K when it is small. When Re is large, the effect of the electrical body forces becomes important, especially when κ is not large. It is known from Eq. (31) that $f''(0)/Re$ and $f''(1)/Re$ are the main parts of the local skin friction coefficients $C_{fx\mathrm{l}}$ and $C_{fx\mathrm{u}}$, respectively. As shown in Fig. 9, $f''(0)/Re$ increases gradually as Re grows for both cases of $\kappa = 3$ and $\kappa = 20$. On the contrary, $f''(1)/Re$ decreases consecutively as Re increases for both cases of $\kappa = 3$ and $\kappa = 20$, as displayed in Fig. 10. For both $f''(0)/Re$ and $f''(1)/Re$, the effects of κ become significant when Re is sufficiently large. As seen in Fig. 11, E_{s} reduces gradually as Re enlarges, particularly, the reduction rate for $\kappa = 3$ is faster than that for $\kappa = 20$. Physically, when κ is appropriately small, the electrostatic potential affects the whole cross-section of the channel. In this case, κ plays an equally important role in the reduction of E_{s} as Re does. When κ is sufficiently large, its effect on the flow is negligible. Re becomes the dominant factor for the decrease of E_{s}.

The effects of G_1 on the various physical quantities of the flow have been shown in Table 2 and Table 3. It can be seen that K and $f''(0)$ decrease as G_1 grows, but $f''(1)$ and E_{s} rise as G_1 increases. Physically, G_1 is related to the electrical strength whose enlargement results in the increase of the electric potential. Since the pressure gradient caused by the electrostatic

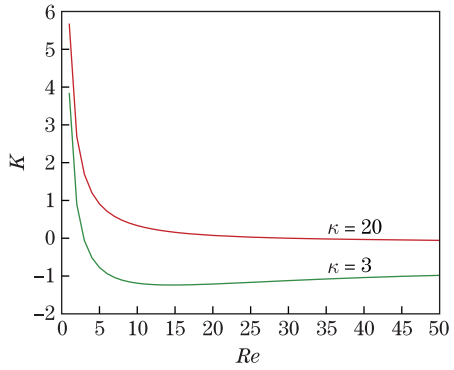

Fig. 8 Dependence of pressure constant K on Re when $G_1 = 100$

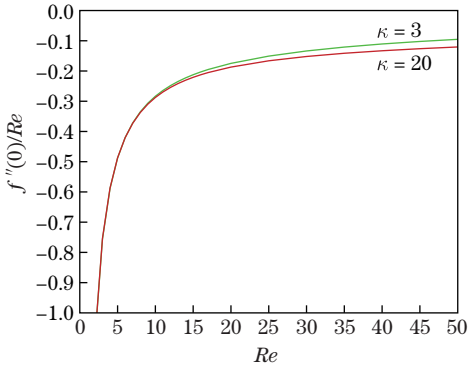

Fig. 9 Variation of $f''(0)$ for local skin frictional coefficient on lower wall along Re when $G_1 = 100$

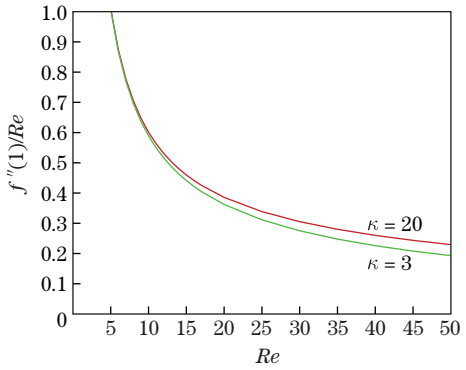

Fig. 10 Variation of $f''(0)$ for local skin frictional coefficient on upper wall along Re when $G_1 = 100$

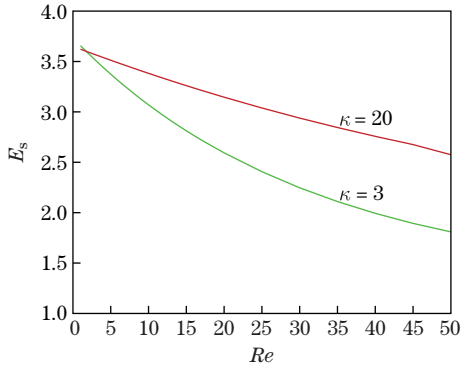

Fig. 11 Dependence of stream potential E_s on Re at $G_1 = 100$

Table 2 Various physical quantities under different values of G_1 when $Re = 5$ and $\kappa = 3$

G_1	$\Phi'(0)$ (exact)	$\Phi'(0)$	K	$f''(0)$	$f''(1)$	E_s
1	−2.715 444 8	−2.715 444 8	0.975 678 8	−1.788 124 2	4.430 843 6	0.036 842 5
10	−2.715 444 8	−2.715 444 8	0.803 452 9	−1.852 257 6	4.489 727 7	0.365 370 0
20	−2.715 444 8	−2.715 444 8	0.615 379 4	−1.922 274 5	4.554 006 7	0.724 070 2
50	−2.715 444 8	−2.715 444 8	0.071 028 8	−2.124 823 1	4.739 916 1	1.761 940 4
100	−2.715 444 8	−2.715 444 8	−0.775 041 6	−2.439 330 8	5.028 466 8	3.374 091 1
150	−2.715 444 8	−2.715 444 8	−1.552 714 6	−2.728 083 6	5.293 258 2	4.854 859 5
200	−2.715 444 8	−2.715 444 8	−2.269 996 2	−2.994 133 7	5.537 119 8	6.219 743 6

Table 3 Various physical quantities under different values of G_1 when $Re = 5$ and $\kappa = 20$

G_1	$\Phi'(0)$ (exact)	$\Phi'(0)$	K	$f''(0)$	$f''(1)$	E_s
1	−19.999 999 9	−19.999 999 9	0.994 090 3	−1.787 680 0	4.430 687 7	0.036 235 6
10	−19.999 999 9	−19.999 999 9	0.986 004 5	−1.848 222 3	4.488 538 3	0.361 318 2
20	−19.999 999 9	−19.999 999 9	0.977 068 9	−1.915 086 6	4.552 428 3	0.720 344 0
50	−19.999 999 9	−19.999 999 9	0.950 565 2	−2.113 160 8	4.741 683 2	1.783 882 0
100	−19.999 999 9	−19.999 999 9	0.907 377 8	−2.435 122 6	5.049 282 2	3.512 568 1
150	−19.999 999 9	−19.999 999 9	0.865 378 7	−2.747 284 6	5.347 486 1	5.188 575 4
200	−19.999 999 9	−19.999 999 9	0.824 520 1	−3.050 086 5	5.636 717 9	6.814 270 3

potential is opposite to that caused by the upper stretching wall, the increase of G_1 leads to the reduction of K. On the other hand, the electrical body force is along the same direction of the viscous force near the upper wall of the channel. As a result, $f''(1)$ enhances as G_1 increases. Due to the conservation of mass flux, $f''(0)$ has to diminish as G_1 grows. Obviously, the increase of the electrostatic potential is helpful to increase E_s. From these tables, we also notice that all these physical quantities vary almost linearly with G_1 from 0 to 200.

6 Conclusions

In this work, we proposed a mathematical model to describe the liquid flow in a microchannel driven by its upper stretching wall in the combination of electrokinetic effects. Comparing with the traditional models, the unphysical boundary condition of the electrostatic potential in the middle of the channel has been fully eliminated. Our model was solved using the similarity transformation. The accurate analytical approximations were given by the HAM, in which the pressure constant and the integral constant related to the electric potential were solved spontaneously by using the proper boundary conditions on the channel walls. It is expected that our model is consistent with the commonly accepted models in the field of fluid mechanics, and can offer the general and proper way to study the flow phenomena in microchannels.

Acknowledgements This work is supported in part by the Australian Research Council through a Discovery Early Career Researcher Award to Qiang SUN.

References

[1] Qu, W. and Mudawar, I. Experimental and numerical study of pressure drop and heat transfer in a single-phase micro-channel heat sink. *International Journal of Heat and Mass Transfer*, **45**, 2549–2565 (2002)

[2] Vafai, K. and Khaled, A. R. A. Analysis of flexible microchannel heat sink systems. *International Journal of Heat and Mass Transfer*, **48**, 1739–1746 (2005)

[3] Figeys, D. and Pinto, D. Lab-on-a-chip: a revolution in biological and medical sciences. *Analytical Chemistry*, **72**, 330–335 (2000)

[4] Tripathi, D., Sharma, A., and Bég, O. A. Electrothermal transport of nanofluids via peristaltic pumping in a finite micro-channel: effects of Joule heating and Helmholtz-Smoluchowski velocity. *International Journal of Heat and Mass Transfer*, **11**, 138–149 (2017)

[5] Eringen, A. C. Simple microfluids. *International Journal of Engineering Science*, **2**, 205–217 (1964)

[6] Pfahler, J., Harley, J., Bau, H., and Zemel, J. Liquid transport in micron and submicron channels. *Sensors and Actuators A*: *Physical*, **22**, 431–434 (1990)

[7] Mala, G. M., Li, D. Q., and Dale, J. D. Heat transfer and fluid flow in microchannels. *International Journal of Heat and Mass Transfer*, **40**, 3079–3088 (1997)

[8] Mala, G. M., Li, D .Q., Werner, C., Jacobasch, H. J., and Ning, Y. B. Flow characteristics of water through a microchannel between two parallel plates with electrokinetic effects. *International Journal of Heat and Fluid Flow*, **18**, 489–496 (1997)

[9] Ren, L. Q., Qu, W. L., and Li, D. Q. Interfacial electrokinetic effects on liquid flow in microchannels. *International Journal of Heat Mass Transfer*, **44**, 3125–3134 (2001)

[10] Berman, A. S. Laminar flow in channels with porous walls. *Journal of Applied Physics*, **24**, 1232–1235 (1953)

[11] Sellars, J. R. Laminar flow in channels with porous walls at high suction Reynolds numbers. *Journal of Applied Physics*, **26**, 489–490 (1955)

[12] Taylor, G. I. Fluid flow in regions bounded by porous surfaces. *Proceedings of the Royal Society of London Seriers A*, **234**, 456–475 (1956)

[13] Proudman, I. An example of steady laminar flow at large Reynolds number. *Journal of Fluid Mechanics*, **9**, 593–602 (1960)

[14] Shrestha, G. M. Singular perturbation problems of laminar flow in a uniformly porous channel in the presence of a transverse magnetic field. *Quarterly Journal of Mechanics and Applied Mathematics*, **20**, 233–246 (1967)

[15] Skalak, F. M. and Wang, C. Y. On the nonunique solutions of laminar flow through a porous tube or channel. *SIAM Journal on Mathematical Analysis*, **34**, 535–544 (1978)

[16] Brady, J. F. and Acrivos, A. Steady flow in a channel or tube with an acceleration surface velocity: an exact solution to the Navier-Stokes equations with reverse flow. *Journal of Fluid Mechanics*, **112**, 127–150 (1981)

[17] Brady, J. F. Flow development in a porous channel and tube. *Physics and Fluids*, **27**, 1061–1067 (1984)

[18] Watson, E. B. B., Banks, W. H. H., Zaturska, M. B., and Drazin, P. G. On transition to chaos in two-dimensional channel flow symmetrically driven by accelerating walls. *Journal of Fluid Mechanics*, **212**, 451–485 (1990)

[19] Dauenhauer, E. C. and Majdalani, J. Exact self-similarity solution of the Navier-Stokes equations for a porous channel with orthogonally moving walls. *Physics of Fluids*, **15**, 1485–1495 (2003)

[20] Liao, S. J. *Beyond Perturbation*: *Introduction to the Homotopy Analysis Method*, Chapman & Hall/ CRC Press, Boca Raton (2003)

[21] Chung, T. J. *Computational Fluid Dynamics*, Cambridge University Press, Cambridge (2002)

[22] Hunter, R. J. *Zeta Potential in Colloid Science*: *Principles and Applications*, Academic Press, New York (1981)

[23] Burgreen, D. and Nakache, F. R. Electrokinetic flow in ultrafine capillary slits. *Journal of Physical Chemistry B*, **68**, 1084–1091 (1964)